Hindawi
Geofluids
Volume 2022, Article ID 8522795, 10 pages
https://doi.org/10.1155/2022/8522795

Research Article

Experimental Study on Uniaxial Compression Fracture Process of Marble Specimens with Circular Holes with Different Diameters

Peng Yan-yan,[1,2] **Xing Ming-hong**,[1,2] **Lin Qun-chao**,[1,2] **and Guo Peng-fei**[1,2]

[1]*School of Civil Engineering, Shaoxing University, Shaoxing 312000, China*
[2]*Key Laboratory of Rock Mechanics and Geological Hazards, Shaoxing 312000, China*

Correspondence should be addressed to Peng Yan-yan; pengyy@usx.edu.cn

Received 21 March 2022; Revised 12 April 2022; Accepted 25 April 2022; Published 21 May 2022

Academic Editor: Hao Wu

After a long period of geological tectonic action, the rock mass develops defects such as pores and fissures of different sizes and scales. The mechanical properties of the rock are largely affected by these discontinuous structures, and there will be obvious stress concentration at the edge of the hole inside the rock. Under the action of concentrated stress, cracks initiate, expand, and penetrate from the edge of the hole to form the final fracture surface and cause instability and failure of the rock mass. In practical engineering, due to the limitation of various factors, it is impossible to conduct uniaxial compressive strength test for each geotechnical engineering. Therefore, the rock in the weak part of the project can be selected as the test specimen before the indoor physical tests. In this paper, the static uniaxial compression test of specimens with circular holes with different diameters is carried out. Digital Image Correlation (DIC) monitoring system is used to observe the test process in real time; then, the data from uniaxial compression test and DIC monitoring test are obtained. At the same time, the macroscopic failure characteristics and crack propagation law of rock specimens are obtained, and the evolution law of strain field during the failure process of rock specimens is also obtained. Meanwhile, Realistic Failure Process Analysis (RFPA) is carried out to verify the accuracy of static uniaxial compression physical tests numerically. Physical tests show that the uniaxial compressive strength of marble specimens with circular holes and the dispersion of measured peak stress data decrease with the increase of hole diameter. The main failure type of marble specimens with circular holes is tension shear failure; the macroscopic failure zone of the sample, the strain field localization zone, and the maximum shear stress field of the numerical test are distributed in a semi-"X" shape with the hole as the center. The localization zone of the strain field on the specimen is usually the region of crack initiation, propagation, and penetration on the surface of the marble specimens. It also shows that specimen breaks in the radial direction along the y-axis of the circular hole, and cracks connecting both ends of the circular hole and the specimen are generated on the specimen. It is of great theoretical value and practical significance to the influence of the cavities in the rock specimens on the stress and strain characteristics and the initiation, propagation, and penetration modes.

1. Introduction

Mining and underground construction will cause changes in rock stress field, which will lead to rock failure under different stress paths. In order to study the rock failure mechanism and mechanical characteristics under different stress paths, a lot of indoor static test research has been conducted. The indoor physical test based on compression test is the basis of geotechnical engineering and rock mechanics test research. In order to facilitate theoretical research and analysis, the stress state of rock is simplified and the influence of protruding axial pressure on rock failure is considered; uniaxial compression test is used to study the failure mechanism and related mechanical characteristics of rock specimens [1–5].

Based on the quasistatic uniaxial compression test, Yang et al. [6], Li et al. [7], Xiong et al. [8], Roan and Vemaganti [9] studied and analyzed the effect of different crack numbers, crack lengths, and inclination on the uniaxial compressive strength and elastic modulus of rock samples and analyzed the crack growth order and its related stress and strain curves. Bobet and Einstein [10] studied the whole

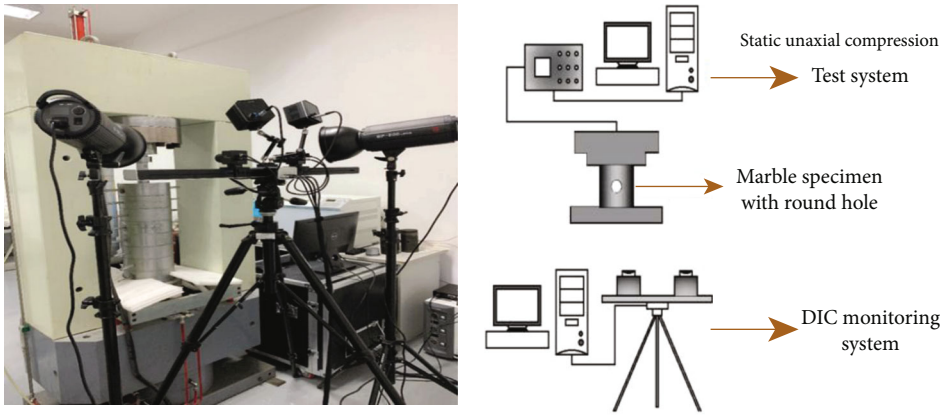

(a) Construction of test equipment (b) Name of each part of test equipment

Figure 1: Schematic diagram of uniaxial compression test system and DIC monitoring system: (a) construction of test equipment; (b) name of each part of test equipment.

process of crack initiation, propagation, and penetration of prefabricated double-fissure gypsum specimens under uniaxial loading. Ko et al. [11] performed uniaxial compression tests on prefabricated double-cracked gypsum specimens. Wing cracks and secondary cracks were observed during the failure process of the specimens. Six failure modes of the specimens were summarized. Park and Bobet and Li et al. [12–14] studied the formation and propagation of cracks on multicracked gypsum specimens under uniaxial compression. Three different types of cracks, wing crack, parallel secondary crack, and inclined secondary crack, and seven different crack penetration types were observed.

Rock is a nonhomogeneous medium, and its macrofracture failure under uniaxial compression is induced by the interaction and aggregation of microcracks [15, 16]. Rock fracture process and destabilization failure results closely related to rock engineering disasters are mostly studied and understood by applying simple static load tests on small rock samples in laboratory physical tests [17–21]. The fracture process and destabilization of rock specimens are related to the inhomogeneity of rock material itself. The observation of nonlinear phenomena during rock fracture is achieved using existing techniques, such as the observation of stress, strain field evolution during fracture of rock specimen, self-organized critical phenomena of rock specimens during the microfracture evolution stage, and stress mutation [22–25]. The application of numerical simulation methods in rock mechanics and engineering practice is becoming more and more common. The Rock Fracture Process Analysis (RFPA) numerical simulation software is developed based on the basic theory of microdamage mechanics, which can track the rock fracture process and fully consider the inhomogeneity of engineering materials such as rock. For the function of numerical analysis of crack propagation and penetration, RFPA adopts the numerical calculation and analysis method of material fracture process based on finite element stress analysis and statistical damage theory which can effectively simulate the whole process of progressive fracture failure and destabilization of rock material [26–30]. One of the main features of this method is to investigate the nonuniformity of rock material. RFPA software has been applied in the aspects of rock burst mechanism, rock movement, pillar destruction, and interaction between cracks. It is an advanced method for numerical analysis of the whole fracture process of rock material and specimens, which simulates nonlinearity by means of material nonuniformity and simulates noncontinuous medium mechanics by means of continuum mechanics. Therefore, RFPA has a good advantage in studying rock mass cracks and can better reflect the discontinuity of structural plane. Therefore, DIC to monitor the failure process of marble specimens with different diameters under uniaxial compression, and RFPA software to simulate and analyze the crack propagation process [31–34].

2. Brief Description of Test Scheme

2.1. Brief Description of Test Equipment. In this paper, the static uniaxial compression test adopts the uniaxial compression test system. The test system has the functions of timely presenting the relationship curves between force and time, force and displacement, displacement and time, stress and time, and strain and time. During the test, multilevel loading can be set in the vertical and horizontal directions. The test system can calculate Poisson's ratio and elastic modulus and automatically calculate relevant mechanical parameters. The static uniaxial compression test in this paper is monitored by DIC monitoring system at the same time. Two CCD cameras are used to capture and generate images in the whole process of the deformation process of the subject so as to obtain the relevant test data such as full field three-dimensional displacement, contour, and strain of the subject. The system can quickly measure, record, and analyze the deformation degree of the subject, form a detailed test data analysis report, and complete a comprehensive and detailed analysis of the behavior law of the test object under static uniaxial compression. The construction of uniaxial compression test system and monitoring system is shown in Figure 1.

Table 1: Information of rock specimen in static uniaxial compression physical test.

Specimen type	Number	Specimen diagram	Dimensions	$H \times \Phi$ (mm)	$a \times b$ (mm)
Prefabricated round hole test piece	JTDZ1-1		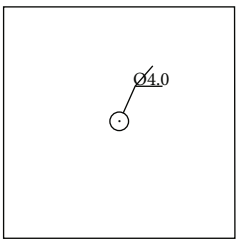	50.32 × 50.08	4.05
	JTDZ1-2			49.81 × 50.12	4.12
	JTDZ1-3			49.78 × 49.89	3.95
	JTDZ2-1		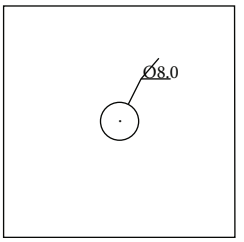	49.92 × 50.05	8.16
	JTDZ2-2			50.16 × 50.21	8.13
	JTDZ2-3			49.83 × 50.11	8.03
	JTDZ3-1		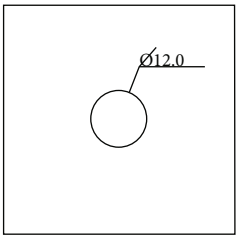	49.88 × 50.13	12.11
	JTDZ3-2			49.56 × 50.04	12.05
	JTDZ3-3			50.15 × 49.96	11.98
	JTDZ4-1		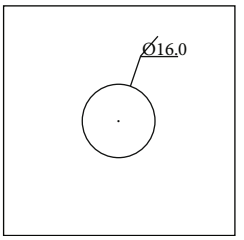	49.67 × 50.23	16.23
	JTDZ4-2			50.12 × 49.68	16.08
	JTDZ4-3			50.07 × 49.72	15.87

Table 1: Continued.

Specimen type	Number	Specimen diagram	Dimensions	$H \times \Phi$ (mm)	$a \times b$ (mm)
	JTDZ5-1 JTDZ5-2 JTDZ5-3		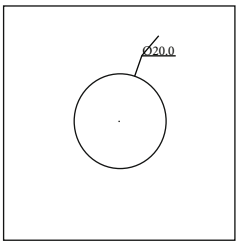	50.14 × 50.13 50.43 × 49.63 49.77 × 50.29	19.96 20.06 20.11

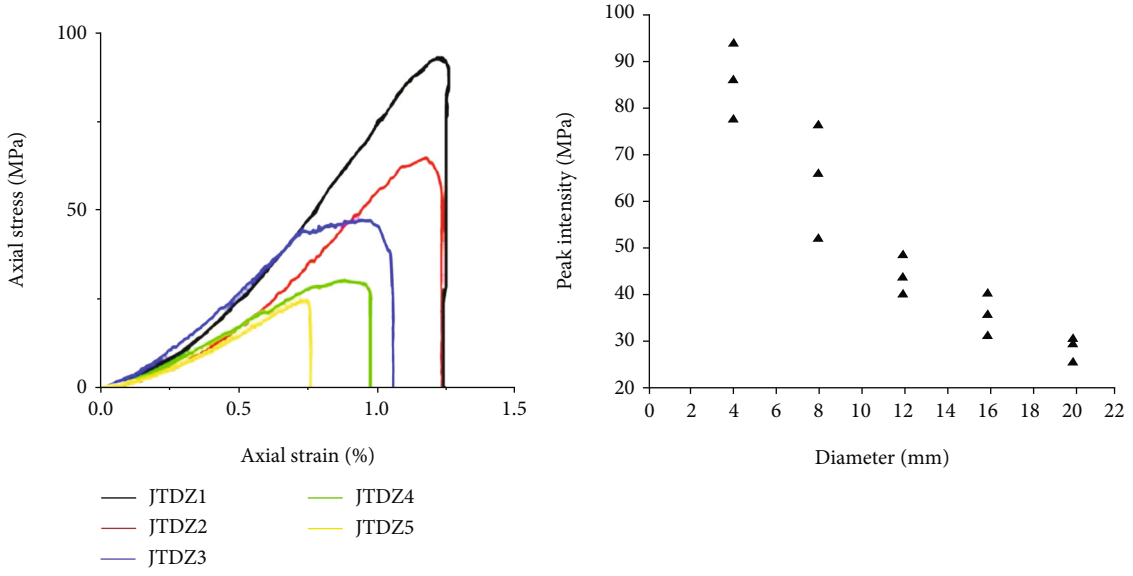

(a) JTDZ1-5

(b) Peak stress of test piece JTDZ1-1~5-3

Figure 2: Axial stress-strain relationship curve and peak stress scatter plot of circular open marble specimens: (a) JTDZ1-5; (b) peak stress of test piece JTDZ1-1~5-3.

2.2. Preparation and Scheme of Static Uniaxial Compression Test

2.2.1. Preparation of Test Piece. The marble used in this paper is collected from the surrounding rock of a mining area in Xuzhou. The specimen is white and dense in appearance and sugar-like in cross section and has a density of 2652 kg/m^3. The main mineral components are dolomite and calcite. Cylindrical specimens with circular holes of different diameters were prepared from the collected marble, and uniaxial compression tests were carried out on the stress and deformation of natural rock holes in mining engineering. The diameter and height of the rock samples are 50.00 mm, and the unevenness and nonperpendicularity of the machined surface are less than 0.02 mm. Five kinds of circular holes with different diameters are prefabricated at the geometric center of the cylinder sample. The diameters of circular holes are 4.00 mm, 6.00 mm, 12.00 mm, 16.00 mm, and 20.00 mm, respectively. The relevant specimen materials are shown in Table 1 below.

2.2.2. Static Uniaxial Compression Test Scheme. Uniaxial compression test system is used to test samples with round holes. The loading mode is set to displacement loading mode, and the loading rate is set to 0.10 mm/min. In addition, DIC monitoring platform system is built to perform real-time monitoring.

3. Results and Analysis

3.1. Stress-Strain Curve of Specimen during Uniaxial Compression Failure

3.1.1. Stress-Strain Curve of Marble Specimen with Round Hole. The complete white marble specimens are prefabricated with round holes of different sizes and then tested under the condition of static uniaxial compression. The stress-strain curve is shown in Figure 2 below.

With different diameters of circular holes as variables, each set of test includes three specimens for each selected

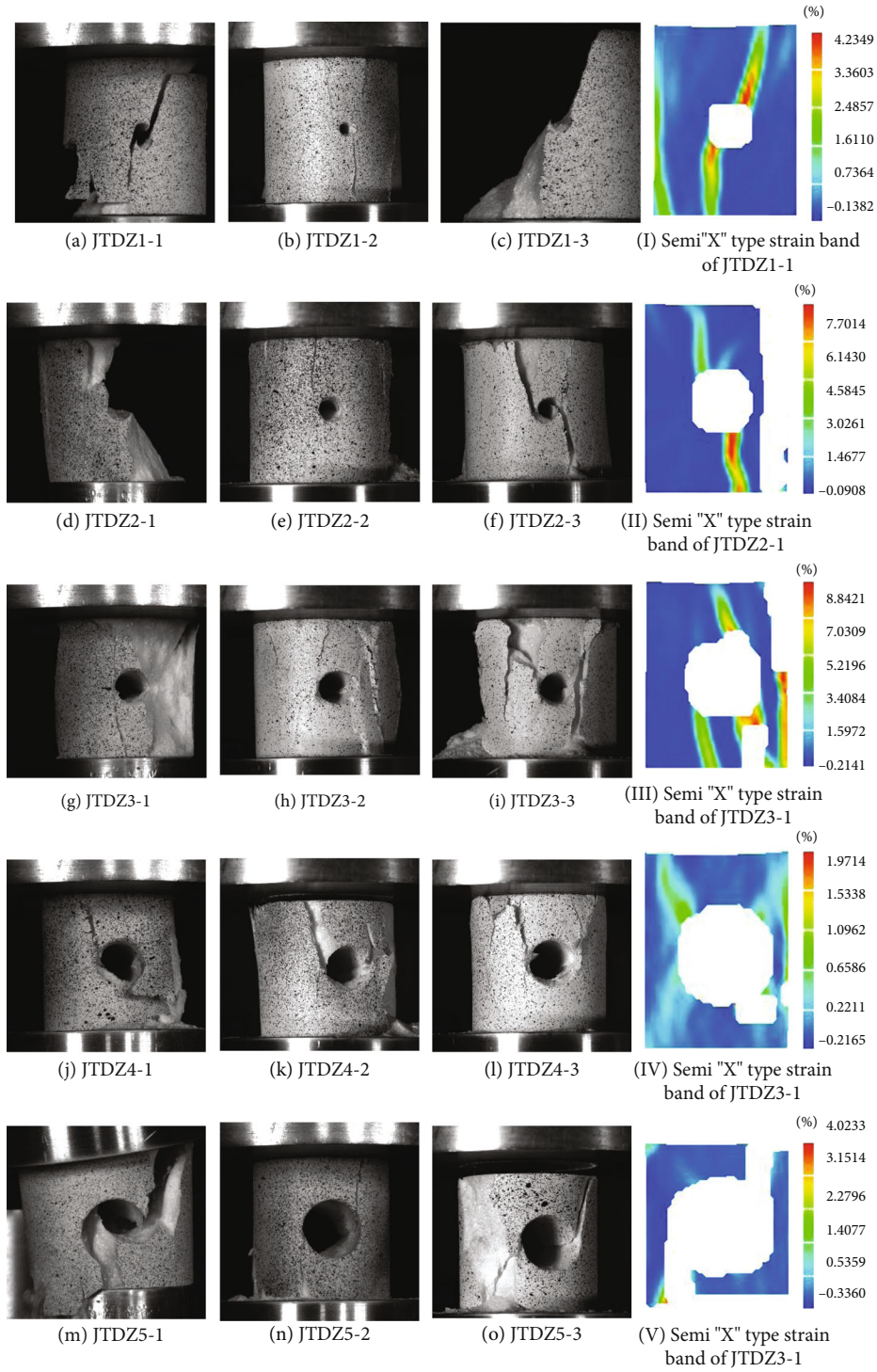

Figure 3: Failure characteristic diagram and x-direction strain cloud diagram of uniaxial compression specimen with circular hole.

diameter. Static uniaxial compression tests are performed to obtain the stress-strain curve of the specimen with circular holes, as shown in Figure 2. The shape and change trend of the stress-strain curve of the same group of specimens with the same diameter holes are basically the same, but due to the heterogeneity of the rock specimen itself, the peak stress of the same group of specimens will be different. Figure 3(b) shows the relationship between the peak stress and the diameter of the prefabricated hole in the test results of each group of specimens. The law shows that as the prefabricated aperture increases, the dispersion of the measured peak stress of the same group of specimens will be smaller. The test results also show that the stress-strain curve of the rock specimen is concave in the initial compaction stage, and the microcracks inside the specimen are closed at this time, and the specimen is compacted. With the gradual

Table 2: Table of mesoscopic uniaxial compressive strength of marble specimens with open circular holes.

Specimen type and number		Macroscopic uniaxial compressive strength (MPa)	Mesouniaxial compressive strength (MPa)
Prefabricated round hole test piece	JTDZ1	87	140
	JTDZ2	66	106
	JTDZ3	44	71
	JTDZ4	35	56
	JTDZ5	28	45

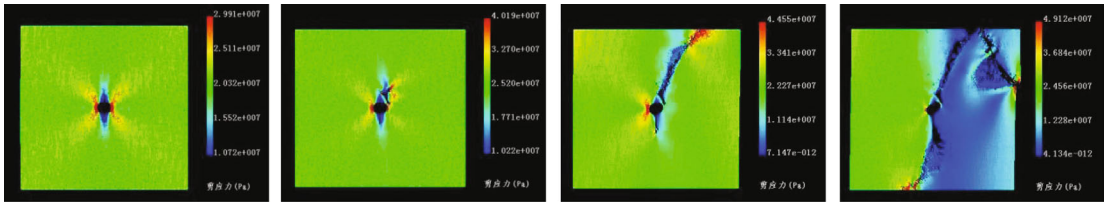

(a) Maximum shear stress nephogram of JTDZ1 uniaxial compression fracture mode

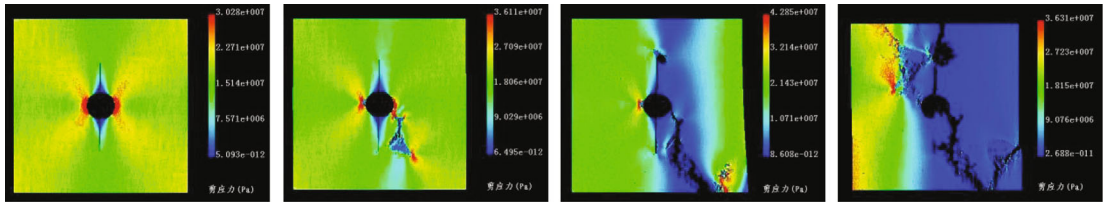

(b) Maximum shear stress nephogram of JTDZ2 uniaxial compression fracture mode

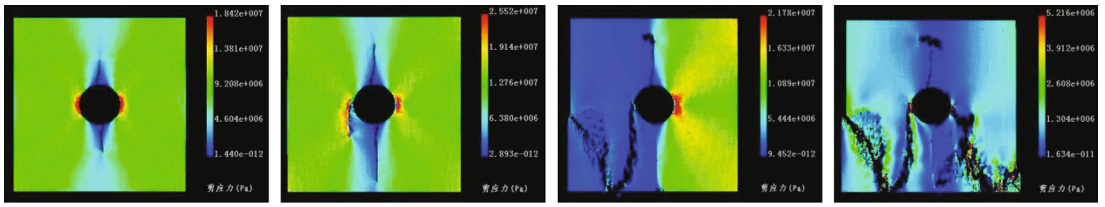

(c) Maximum shear stress nephogram of JTDZ3 uniaxial compression fracture mode

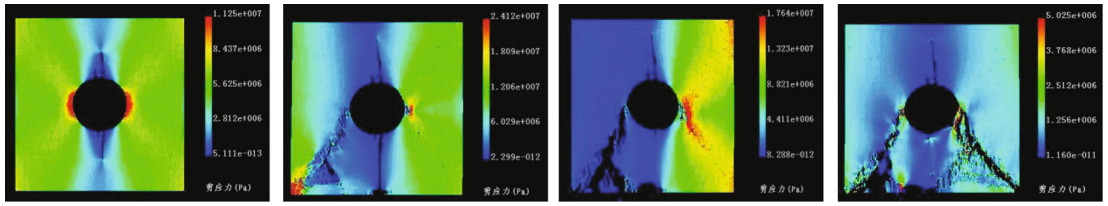

(d) Maximum shear stress nephogram of JTDZ4 uniaxial compression fracture mode

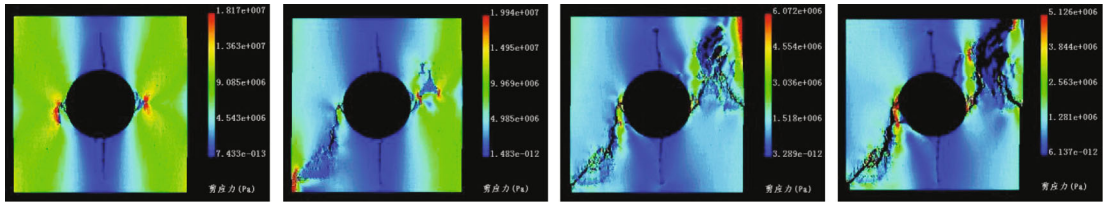

(e) Maximum shear stress nephogram of JTDZ5 uniaxial compression fracture mode

Figure 4: Maximum shear stress nephogram of uniaxial compression fracture mode.

increase of the axial strain of the specimen and the gradual increase of the axial stress, the curve enters the linear elastic deformation stage. At this time, the stress-strain curve is close to a straight line. As the axial strain continues to increase, the curve enters the stage of unstable crack propagation. The specimen changes from elastic stage to plastic

stage, microcracks develop continuously, the surface of the specimen breaks, and the volume of the specimen changes from compression to expansion. After the peak stress, the interior of the specimen has been damaged. Cracks expand in a short period of time. The cracks combine and intersect with each other to form macroscopic cracks and extend. Then, a cliff-like dip of the stress-strain curve appears. This could be due to the brittle physical properties of the rock specimen itself. According to the above stress-strain curves, it can also be seen that the peak strength of the specimen decreases with the increase of hole diameter, indicating that the bearing capacity of the specimen will decrease with the increase of hole size. The average uniaxial compressive strengths of JTDZ1-5 are 87.8 MPa, 66.4 MPa, 44.2 MPa, 35.6 MPa, and 28.7 MPa, respectively (the first to fifth groups of specimens with circular holes).

3.1.2. Failure Characteristics and Strain Field Analysis of Marble Specimens with Round Holes. The failure characteristics of the specimen with a hole diameter of 4 mm under uniaxial compression are shown in Figures 3(a)–3(c). As shown in Figure 3(a), a semi-X-shaped macroscopic failure crack is generated in the specimen JTDZ1-1, and the final failure state of specimen JTDZ1-3 is shown in Figure 3(c). The specimen itself is damaged due to the penetration of semi-"X" type macro-failure cracks along the side of the specimen, and the failure form is tension shear failure. The failure characteristics of the specimens JTDZ2-1, JTDZ2-1, and JTDZ2-3 with a circular hole diameter of 8 mm shown in Figures 3(d)–3(f) are similar to those of the specimen with a circular hole diameter of 4 mm, with the same tensile-shear failure patterns and similar microcrack shape. The specimens with holes of 12 mm diameter shown in Figures 3(g)–3(i) have two obvious vertical through cracks on the side. In the later stage of the test, the specimen collapses along the crack direction, accompanied by a certain noise, and the fragments of the specimen fly around at the same time. The main form of specimen failure is tensile shear failure. As shown in Figures 3(j)–3(l), the main fracture state of the specimens JTDZ4-1-JTDZ4-3 with a circular hole diameter of 16 mm is still a semi-"X"-type macrofailure crack penetrating along the side of the specimen, and the specific failure form is still tension shear failure. As shown in Figures 3(m)–3(o), the fracture state of the specimens JTDZ4-1-JTDZ4-3 with a circular hole diameter of 20 mm is still along one side of the specimen and exhibits a semi-"X" shape; also, the failure type is pull-shear failure. The fracture failure process of the specimen can be divided into the following development and evolution stages: the initial compaction stage of the specimen, the linear elastic deformation stage, the stable crack propagation stage of the specimen, the unstable crack propagation stage, and the post peak stage. In the initial loading stage of static uniaxial compression test, the cracks and holes in the rock specimen are still hard to be observed; also, it is difficult to directly observe the original structure in the rock specimen, which is continuously compacted under the influence of rising uniaxial pressure. At this time, there will be no new cracks in the specimen; this stage is called the initial compaction stage. During the continuous increase of loading pressure, the marble specimen with round holes continues to undergo elastic deformation, and new small cracks appear around the round hole. This stage is the stage of linear elastic deformation. Then, the crack extends smoothly to the top and bottom of the specimen, and the surface of the rock specimen also forms signs of debris spalling. This stage is called the stable crack propagation stage. When the uniaxial pressure of marble specimen exceeds a certain degree, the crack on its surface begins to expand unevenly and rapidly. At this time, the rock specimen enters the stage of unstable crack propagation. With the penetration of cracks in the specimen, the specimen will produce brittle failure, and the specimen will enter the stage of brittle failure. After the brittle failure of rock specimen, the specimen may enter the postpeak stage. In Figure 3, the x -direction strain field of the specimen under uniaxial compression is also given. The cloud image shows that the strain field localization zone is located around the circular hole of the sample and presents a semi-"X" distribution centered on the circular hole. The localization zone of the strain field is usually the initiation, propagation, and penetration zone of surface crack.

3.2. Evolution of Uniaxial Compressive Stress Field Based on RFPA. The above analysis reveals the relevant stress-strain curves, failure characteristics, and evolution of strain field of marble specimens with circular holes under uniaxial compression. In order to verify the physical test results, finite element analysis is carried out using RFPA software. After the macrouniaxial compressive strength obtained from physical test is transformed into the microuniaxial compressive strength required by RFPA software, the grid is established. Then, the numerical test model is constructed after inputting the geometric parameters of the model and a series of basic mechanical parameters. The set loading conditions are consistent with the physical test, and the physical test is simulated. The stress field distribution diagram of the specimen in the process of uniaxial compression fracture is obtained. In this paper, the calculation input values of the mesostrength and mesoelastic modulus used in the numerical simulation test can be converted from the macroelastic modulus and macrostrength obtained by the physical test according to the fitting formula. The formula is as follows:

$$\begin{aligned} \frac{f_{\text{macro}}}{f_{\text{meso}}} &= 0.2602 \ln m + 0.0233 (1.2 \le m \le 50), \\ \frac{E_{\text{macro}}}{E_{\text{meso}}} &= 0.1412 \ln m + 0.6476 (1.2 \le m \le 10). \end{aligned} \tag{1}$$

The converted numerical parameters are shown in Table 2.

Figure 4 shows the distribution of the maximum shear stress field during the static uniaxial compression fracture process of the rock specimen obtained from the numerical test. It can be seen from Figure 4 that the crack fracture form of the numerical sample is consistent with the semi-"X"-type

macrofailure crack in the physical test shown in Figure 3. From the maximum shear stress nephogram of numerical simulation, the fracture process of the specimen can be revealed in more detail. In Figure 4(a), the fracture process shows that due to the predrilled holes of the specimen, the maximum shear stress field is distributed in a semi-"X" shape along the periphery of the circular hole, and the specimen first breaks along the radial direction of the y-axis of the circular hole, and cracks extend from both ends of the circular hole to both ends of the specimen. When the shear stress is released, the color of the cloud image becomes light and blue, which means that this part of the specimen becomes low. The upper right area of the round hole is broken, and the blue area in the cloud image extends. The crack in the lower left area of the round hole begins to appear, and the crack extends along the semi-"X" shape to the bottom of the specimen. The crack fracture form of the numerical test in Figure 4(a) corresponds to that in Figures 3(a)–3(c), with a semi-"X"-type macrofailure crack. With the increase of the diameter of the circular hole, there is a crack penetrating through the specimen along the circular hole diameter of the y-axis in Figure 4(b), and the color of the stress nephogram changes from green to blue after fracture, indicating that the process is accompanied by the release of shear stress. The crack continues to expand and extend to the bottom of the specimen, and a small round hole appears at the crack end and extend from the upper end of the round hole along the y-axis. The crack at the upper end of the round hole on the y-axis continues to expand and extend, the small round hole continues to expand, and the stress in the upper left area of the round hole is concentrated, which is a sign of crack generation. Consistent with the physical test, the cracks in the upper left and lower right areas of the round hole of the test piece form a semi-"X"-type macrofailure crack, as shown in Figures 3(d) and 3(e).The diameter of the circular hole in the numerical model continues to expand, and the simulation results are consistent with the previous ones. The stress concentration first appears on the left and right sides of the circular hole, and there are small cracks passing through the specimen along the direction of the circular hole of the y-axis. The new crack first appears at the lower left of the round hole. With the operation of the model, the crack develops and extends to the bottom of the test piece and the small crack passing through the test piece in the direction of the circular aperture of the y-axis. Also, further propagation and extension develop until a small round hole is formed, as shown in the middle and later stages of Figures 4(b) and 4(c).The crack propagation direction at the bottom rotates; also, the crack extends to the upper part of the test piece and stops growing at the left end of the contact test piece, as shown in the middle and later stages of Figures 4(c) and 4(d). The crack form of the numerical specimens JTDZ3 and JTDZ4 is roughly semi-"X," which is consistent with that in the physical test, and its failure type is still compression shear failure. The crack form and stress field distribution of the numerical simulation results of specimen JTDZ5 are similar to those of specimen JTDZ1 and JTDZ2, and the results are also consistent with the physical test.

4. Conclusion

Uniaxial compression test is carried out on specimens with round holes, and the stress-strain curve of the specimen is obtained. At the same time, the macroscopic failure characteristics of the marble samples under uniaxial compression are obtained, and the uniaxial compression process of the specimen is monitored through the DIC system. Then, combined with RFPA numerical simulation software, the uniaxial compression physical test is verified. The following conclusions are obtained from physical and numerical experiments:

(1) The uniaxial compressive strength and the discreteness of the measured peak stress of the marble specimen with circular hole decrease with the increase of the hole diameter

(2) The failure type of marble specimens with round hole is mainly tension shear failure, and the macrofailure zone presents a semi-"X" distribution centered on the round hole

(3) By collecting the speckle images during the uniaxial compression test, the evolution nephogram of the strain field during the uniaxial compression failure of the specimen is obtained. The cloud image shows that the strain field localization band is located around the hole of the sample and is in a semi-"X" shape. The localization region of strain field is usually the surface crack initiation, propagation, and penetration region

(4) In the numerical simulation test of uniaxial compression, due to the predrilled holes of the specimen, during the loading process, the maximum shear stress field is distributed in a semi-"X" shape along the periphery of the circular hole, and the specimen first breaks in the radial direction along the y-axis of the circular hole. Finally, a crack extending from both ends of the circular hole to both ends of the specimen is generated, which is consistent with the semi-"X"-type macrofailure crack in the physical test

Data Availability

The data reported in this article are available from the corresponding author upon request.

Conflicts of Interest

The authors declare no conflicts of interest.

Authors' Contributions

The manuscript is approved by all authors for publication.

Acknowledgments

This is supported by the National Natural Science Foundation of China (No. 41702381) and Zhejiang Public Welfare Technology Research Project/Social Development (No. LGF20D020002).

References

[1] Y. T. Yin, G. L. Li, Y. Liu, X. Jiang, and W. Luan, "Research on uniaxial compression of jointed rock mass based on numerical simulation," *IOP Conference Series: Earth and Environmental Science*, vol. 804, no. 2, p. 022053, 2021.

[2] Z. X. Liu, G. M. Zhao, X. R. Meng, R. Zhang, D. Chunliang, and W. Xu, "Energy analysis method for uniaxial compression test of sandstone under static and quasi-dynamic loading rates," *Advances in Materials Science and Engineering*, vol. 2021, Article ID 9933243, 11 pages, 2021.

[3] M. C. He, "Conception system and evaluation indexes for deep engineering," *Chinese Journal of Rock Mechanics and Engineering*, vol. 24, no. 16, pp. 2854–2858, 2005.

[4] M. C. He, H. P. Xie, S. P. Peng, and Y. D. Jiang, "Study on rock mechanics in deep mining engineering," *Chinese Journal of Rock Mechanics and Engineering*, vol. 24, no. 16, pp. 2803–2813, 2005.

[5] Z. Y. Song, "Experimental study on the characteristics of acoustic emission source of rock under uniaxial compression," *IOP Conference Series: Earth and Environmental Science*, vol. 791, no. 1, article 012003, 2021.

[6] S. Q. Yang, Y. H. Dai, L. J. Han, and Z. Q. Jin, "Experimental study on mechanical behavior of brittle marble samples containing different flaws under uniaxial compression," *Engineering Fracture Mechanics*, vol. 76, no. 12, pp. 1833–1845, 2009.

[7] P. Li, C. R. Siviour, and N. Petrinic, "The effect of strain rate, specimen geometry and lubrication on responses of aluminium AA2024 in uniaxial compression experiments," *Experimental Mechanics*, vol. 49, no. 4, pp. 587–593, 2009.

[8] X. Xiong, J. Dai, Y. Ouyang, and P. Shen, "Experimental analysis of control technology and deformation failure mechanism of inclined coal seam roadway using non-contact DIC technique," *Scientific Reports*, vol. 11, no. 1, pp. 1–23, 2021.

[9] R. Esra and V. Kumar, "The nonlinear material properties of liver tissue determined from no-slip uniaxial compression experiments," *Journal of Biomechanical Engineering*, vol. 129, no. 3, pp. 450–456, 2007.

[10] A. Bobet and H. H. Einstein, "Fracture coalescence in rock-type materials under uniaxial and biaxial compression," *International Journal of Rock Mechanics and Mining Sciences*, vol. 35, no. 7, pp. 863–888, 1998.

[11] T. Ko, H. Einstein, and J. Kemeny, "Crack coalescence in brittle material under cyclic loading," in *Proceedings of the 41st U.S. Rock Mechanics Symposium - ARMA's Golden Rocks 2006 - 50 Years of Rock Mechanics*, Golden, Colorado, 2006.

[12] C. H. Park and A. Bobet, "Crack coalescence in specimens with open and closed flaws: a comparison," *International Journal of Rock Mechanics and Mining Sciences*, vol. 46, no. 5, pp. 819–829, 2009.

[13] C. H. Park and A. Bobet, "Crack initiation, propagation and coalescence from frictional flaws in uniaxial compression," *Engineering Fracture Mechanics*, vol. 77, no. 14, pp. 2727–2748, 2010.

[14] C. W. Li, Q. F. Wang, D. H. Ai, L. Dong, and F. Wang, "Study of EMR and AE during coal fracture under quasi-static uniaxial compression load," *Journal of Environmental and Engineering Geophysics*, vol. 22, no. 4, pp. 385–394, 2017.

[15] J. B. Zhu, T. Zhou, Z. Y. Liao, L. Sun, X. B. Li, and R. Chen, "Replication of internal defects and investigation of mechanical and fracture behaviour of rock using 3D printing and 3D numerical methods in combination with X-ray computerized tomography," *International Journal of Rock Mechanics and Mining Sciences*, vol. 106, pp. 198–212, 2018.

[16] X. F. Wang, Z. G. Xia, P. Li, and H. Liu, "Numerical study on strength and failure behavior of rock with composite defects under uniaxial compression," *Energies*, vol. 14, no. 15, pp. 4418–4418, 2021.

[17] B. Liu, Y. X. Zhao, C. Zhang, J. Zhou, Y. Li, and Z. Sun, "Characteristic strength and acoustic emission properties of weakly cemented sandstone at different depths under uniaxial compression," *International Journal of Coal Science & Technology*, vol. 8, no. 6, pp. 1288–1301, 2021.

[18] Y. L. Chen, J. P. Zuo, D. J. Liu, Y. Li, and Z. Wang, "Experimental and numerical study of coal-rock bimaterial composite bodies under triaxial compression," *International Journal of Coal Science & Technology*, vol. 8, no. 5, pp. 908–924, 2021.

[19] H. K. Gao, Q. Wang, B. Jiang, P. Zhang, Z. Jiang, and Y. Wang, "Relationship between rock uniaxial compressive strength and digital core drilling parameters and its forecast method," *International Journal of Coal Science & Technology*, vol. 8, no. 4, pp. 605–613, 2021.

[20] J. Wang, J. X. Yang, F. F. Wu, T. Hu, and S. A. Faisal, "Analysis of fracture mechanism for surrounding rock hole based on water-filled blasting," *International Journal of Coal Science & Technology*, vol. 7, no. 4, pp. 704–713, 2020.

[21] X. S. Guo, T. K. Nian, W. Zhao et al., "Centrifuge experiment on the penetration test for evaluating undrained strength of deep-sea surface soils," *Mining Science and Technology*, vol. 32, no. 2, pp. 363–373, 2022.

[22] C. Zou and H. Q. Li, "Combined numerical and experimental studies on the dynamic and quasi-static failure modes of brittle rock," *International Journal of Rock Mechanics and Mining Sciences*, vol. 148, p. 104957, 2021.

[23] G. Shi, X. Yang, H. Yu, and C. Zhu, "Acoustic emission characteristics of creep fracture evolution in double- fracture fine sandstone under uniaxial compression," *Engineering Fracture Mechanics*, vol. 210, pp. 13–28, 2019.

[24] Y. Wang, J. Tang, Z. Dai, and T. Yi, "Experimental study on mechanical properties and failure modes of low-strength rock samples containing different fissures under uniaxial compression," *Engineering Fracture Mechanics*, vol. 197, pp. 1–20, 2018.

[25] W. F. Ranson and W. H. Peters, "Digital image techniques in experimental stress analysis," *Optical Engineering*, vol. 21, no. 3, pp. 427–431, 1982.

[26] M. A. Eltaher and A. Wagih, "Micromechanical modeling of damage in elasto-plastic nanocomposites using unit cell representative volume element and cohesive zone model," *Ceramics International*, vol. 46, no. 8, pp. 10469–10480, 2020.

[27] J. Ma, X. L. Li, J. G. Wang et al., "Experimental study on vibration reduction technology of hole-by-hole presplitting blasting," *Geofluids*, vol. 2021, Article ID 5403969, 10 pages, 2021.

[28] J. Leclerc, V.-D. Nguyen, T. Pardoen, and L. Noels, "A micromechanics-based non-local damage to crack transition framework for porous elastoplastic solids," *International Journal of Plasticity*, vol. 127, no. C, pp. 102631–102631, 2020.

[29] M. He, Z. Q. Zhang, J. W. Zhu, N. Li, G. Li, and Y. S. Chen, "Correlation between the rockburst proneness and friction characteristics of rock materials and a new method for rockburst proneness prediction: field demonstration," *Journal of Petroleum Science and Engineering*, vol. 205, article 108997, 2021.

[30] L. Cheng, L. Jianfeng, R. Yi, and L. Y. Liaochao, "Study on very long-term creep tests and nonlinear creep-damage constitutive model of salt rock," *International Journal of Rock Mechanics and Mining Sciences*, vol. 146, article 104873, 2021.

[31] J. Wang, T. Zuo, X. Li, Z. Tao, and J. Ma, "Study on the fractal characteristics of the pomegranate biotite schist under impact loading," *Geofluids*, vol. 2021, Article ID 1570160, 8 pages, 2021.

[32] X. S. Guo, T. K. Nian, D. Wang, and Z. D. Gu, "Evaluation of undrained shear strength of surficial marine clays using ball penetration-based CFD modelling," *Acta Geotechnica*, vol. 35, 2021.

[33] Y. Guansheng Han, R. L. Zhou, Q. Tang, X. Wang, and L. Song, "Infuence of surface roughness on shear behaviors of rock joints under constant normal load and stifness boundary conditions," *Natural Hazards*, vol. 2, pp. 1–19, 2022.

[34] W. Zhong, J. Ouyang, D. Yang, X. Wang, Z. Guo, and K. Hu, "Effect of the in situ leaching solution of ion-absorbed rare earth on the mechanical behavior of basement rock," *Journal of Rock Mechanics and Geotechnical Engineering*, vol. 46, 2021.